OXFORD

Human Molecular Genetics, 2018, Vol. 27, No. 3 505–515

doi: 10.1093/hmg/ddx420
Advance Access Publication Date: 7 December 2017
Original Article

ORIGINAL ARTICLE

Zinc finger protein 274 regulates imprinted expression of transcripts in Prader-Willi syndrome neurons

Maéva Langouët[1,*,†], Heather R. Glatt-Deeley[1,†], Michael S. Chung[1], Clémence M. Dupont-Thibert[1], Elodie Mathieux[1], Erin C. Banda[1], Christopher E. Stoddard[1], Leann Crandall[1] and Marc Lalande[1,2]

[1]Department of Genetics and Genome Sciences, School of Medicine and [2]Institute for Systems Genomics, University of Connecticut, Farmington, CT 06030-6403, USA

*To whom correspondence should be addressed at: Department of Genetics and Genome Sciences, University of Connecticut Health Center, University of Connecticut Stem Cell Institute, Farmington, CT 06030-6403, USA. Tel: +1 8606792323; Fax: +1 8606798345; Email: maeva.langouet@gmail.com

Abstract

Prader-Willi syndrome (PWS) is characterized by neonatal hypotonia, developmental delay and hyperphagia/obesity and is caused by the absence of paternal contribution to chromosome 15q11-q13. Using induced pluripotent stem cell (iPSC) models of PWS, we previously discovered an epigenetic complex that is comprised of the zinc-finger protein ZNF274 and the SET domain bifurcated 1 (SETDB1) histone H3 lysine 9 (H3K9) methyltransferase and that silences the maternal alleles at the PWS locus. Here, we have knocked out *ZNF274* and rescued the expression of silent maternal alleles in neurons derived from PWS iPSC lines, without affecting DNA methylation at the PWS-Imprinting Center (PWS-IC). This suggests that the ZNF274 complex is a separate imprinting mark that represses maternal PWS gene expression in neurons and is a potential target for future therapeutic applications to rescue the PWS phenotype.

Introduction

PWS (MIM 176270), a neurobehavioral disorder of genomic imprinting, is characterized by neonatal hypotonia and failure to thrive during infancy and, subsequently, by obesity, hyperphagia, cognitive disability and behavioral abnormalities. PWS is caused by the absence of a normal paternal contribution to chromosome 15q11-q13, most commonly due to a large deletion (LD) of the ∼5000kb imprinted region or to maternal uniparental disomy (mUPD) of chromosome 15 (1,2). Maternally inherited deletion of the 15q11-q13 imprinted region or paternal UPD causes Angelman syndrome (AS), a disorder characterized by seizures, movement difficulty, cognitive disability and failure to speak (3–5).

The germline imprint of 15q11-q13 is a differentially methylated CG-rich segment, termed the PWS-IC (6–9), located in the first exon of the gene encoding small nuclear ribonucleoprotein polypeptide N (*SNRPN*). *SNRPN* is a bicistronic transcript that also encodes *SNURF* (referred to henceforth as *SNRPN* in this report). In the brain, a long non-coding RNA (*lncRNA*) initiates at upstream (U) exons of SNRPN (Fig. 1A), extends >600kb distally to overlap *UBE3A*, and silences the paternal *UBE3A* allele via an antisense-mediated mechanism (10–18). The PWS *lncRNA* serves as the host gene (HG) to several box C/D class small nucleolar RNAs including the *SNORD116* and *SNORD115* clusters (10,18). There are 30 copies of *SNORD116* in the cluster which has been subdivided into three groups based on DNA sequence similarity (19), Group 1 (*SNOG1, SNORD116 1–9*), Group 2, [*SNOG2, SNORD116 10–24* and Group 3 (*SNOG3, SNORD116 25–30*)]. Moreover, it has been recently shown that loss of *SNORD116* in both human iPSC deletion and mouse models of PWS have a

[†]These authors contributed equally to this work.

Received: August 2, 2017. **Revised:** November 29, 2017. **Accepted:** December 1, 2017

deficiency of prohormone convertase PC1 that may potentially be associated with the neuroendocrine dysfunction in PWS (20,21). These results suggest an association between *SNORD116* deletion and PWS.

Using our PWS and AS iPSC models, we have previously reported that ZNF274 binds to six sites in the maternal copy of the *SNORD116* cluster and, associated in a complex with the histone methyltransferase SETDB1, mediates the deposition of the repressive H3K9me3 chromatin mark on the maternal allele (22–24). Given its putative function in tethering the epigenetic silencing complex to the maternal allele, we have targeted *ZNF274* using CRISPR/Cas9 technology and followed the impact of the knockout on maternal allele expression in PWS-specific iPSCs through the process of neuronal differentiation.

Results

Generation and characterization of *ZNF274* KO lines

In addition to our previously characterized PWS LD iPSCs (25), we generated iPSC lines from a PWS UPD patient (Supplementary Material, Fig. S1B and Table S1D). We performed CRISPR/Cas9-mediated knockout of *ZNF274* in PWS-specific iPSCs in order to determine the impact of ZNF274 depletion on H3K9me3 accumulation at the *SNORD116* locus. The genetic alterations induced by *ZNF274* knockout (*ZNF274* KO) are summarized in Supplementary Material, Table S1C for the PWS LD *ZNF274* KO lines (LD KO1 and LD KO2) and UPD *ZNF274* KO lines (UPD KO1, UPD KO2 and UPD KO3). Karyotypic analysis of the engineered iPSC lines showed no detectable abnormalities (Supplementary Material, Table S1D). We performed routine testing for pluripotency (Supplementary Material, Fig. S1B), and we did not observe any sequence changes within the top potential off-target loci (Supplementary Material, Table S1E).

CRISPR/Cas9-mediated knock out of *ZNF274* depletes H3K9me3 at the *SNORD116* locus in PWS-specific iPSCs

We performed Chromatin ImmunoPrecipitation (ChIP) on the PWS LD and UPD iPSCs and their derivative *ZNF274* KO clones as well as from iPSCs from control individuals (CTRL1 and CTRL2) (22,25–27) and an AS patient with a large deletion of the maternal chromosome 15q11-q13(25) and observed a complete absence of ZNF274 binding to all PWS LD and UPD *ZNF274* KO clones at all the 12 known ZNF274 binding sites tested, demonstrating an efficient *ZNF274* KO (Fig. 1B and Supplementary Material, Fig. S2A). This absence of ZNF274 binding is associated with a marked reduction of H3K9me3 at the six ZNF274 binding sites (BSs) (*SNOG1-BS1* to *SNOG1-BS6*) in all PWS LD and UPD *ZNF274* KO clones, demonstrating the efficient disruption of ZNF274 function at the *SNORD116* locus in our KO iPSC lines. Although we observed a complete absence of the ZNF274 protein at all the known ZNF274 BSs we tested, the level of H3K9me3 was not reduced at the ZNF274 BS in the *ZNF180*.

3'UTR that we used as our reference. The likely explanation is that ZNF274 BSs are most often shared with a second zinc finger protein (ZNF75D) (28). In fact, 89.1% of ZNF274 binding sites in KRAB domain-containing zinc finger protein genes are shared with ZNF75D (28). For example, the 3'UTR of *ZNF180* and *ZNF554* are two target regions bound by both ZNF274 and ZNF75D and we observe little or no effect on H3K9me3 levels at those sites (Supplementary Material, Fig. S2B). The 3'-ends of *ZNF781* and *ZNF90*, on the other hand, are two of the rare sites that are bound only by ZNF274 and, consistent with this observation, we detect a more marked reduction of H3K9me3 for those two BSs (Supplementary Material, Fig. S2B).

The levels of H3K9me3 are also reduced in the PWS LD and UPD *ZNF274* KO clones at *SNOG2* and *SNOG3*, which are *SNORD116* class group 2 and 3 loci (19) located downstream of *SNOG1-BS1 to SNOG1-BS6* (Supplementary Material, Fig. S2C). The spread of H3K9me3 deposition at the maternal-specific *SNOG1* ZNF274 BSs is consistent with our previous observation (22). We observed a concomitant activation of expression of the *SNORD116* host gene Group1 (*116HGG1*) transcript in our *ZNF274* KO PWS LD and UPD iPSCs (Supplementary Material, Fig. S2D). These results suggest that *ZNF274* KO in PWS iPSCs reduces H3K9me3, leading to chromatin de-condensation and partial transcriptional activation of *116HGG1* within the PWS locus.

Impact of *ZNF274* KO on *SNRPN* activation in PWS-specific iPSCs

We also investigated the mechanism by which *ZNF274* KO activates *116HGG1* expression by examining the regulatory elements of the PWS lncRNA. For this, we analysed *SNRPN* transcripts driven by the major promoter in exon 1 and by its alternative upstream exon promoters, U1B and U1A, that drive PWS *lncRNA* predominantly in brain (11,12,14). SNRPN transcripts driven by U1B and U1A skip exon 1 and splice into exon 2 (8,29–31). We assayed for RNAs that splice from exon U4 to exon 2 since the U4 internal exon is included in most *SNRPN* U1B and U1A transcripts (11,12,32). We detected *ZNF274* KO-mediated activation of U4/exon 2 (Fig. 2A) but not of exon 1/exon 2 *SNRPN* transcripts (Fig. 2B), a finding that suggests that the ZNF274 complex represses maternal PWS transcripts through its action on the U1B and U1A promoters rather than the major *SNRPN* exon 1 promoter. Consistent with this suggestion, we detect only partial activation of the *SNRPN* exon 3–4 coding transcript (Fig. 2C) in the absence of SNRPN major exon 1 promoter usage (Fig. 2B). To further understand the impact of *ZNF274* KO on the regulation of *SNRPN* and PWS, we examined DNA methylation in the PWS-IC, which is contained within SNRPN exon 1 (Fig. 2D). In PWS LD iPSCs and their *ZNF274* KO derivatives, we observe almost identical levels of CpG methylation at the maternal PWS-IC (Fig. 2D). These findings are not only consistent with our observation that the maternal *SNRPN* exon 1 promoter is not activated by *ZNF274* KO but suggest, importantly, that ZNF274 is an epigenetic regulator of chromosome 15q11-q13 imprinting that acts independently of the PWS-IC.

ZNF274 KO restores maternal gene expression in PWS neurons

Given that the *SNRPN* exon U1B and U1A are active mainly in the brain (11,12,14), we derived neural progenitor cells (NPCs) and neurons from our iPSC lines to further understand the mechanism of the rescue of maternal PWS transcripts by *ZNF274* KO (Fig. 3). Although *ZNF274* KO increases the expression of maternal *116HGG1* by $\geq$100X in PWS iPSCs (Supplementary Material, Fig. S2D), the levels attained are much lower than those in CTRL iPSC lines for *116HGG1* (Fig. 3A). However, a more robust activation is observed upon neural differentiation with *116HGG1* expression almost reaching control levels in *ZNF274* KO NPCs and attaining or surpassing these in rescued neurons (Fig. 3B and C). *ZNF274* KO in PWS LD and UPD lines results in a marked increase of *116HGG1* expression relative to CTRL lines after 4 weeks of differentiation (Fig. 3B) and

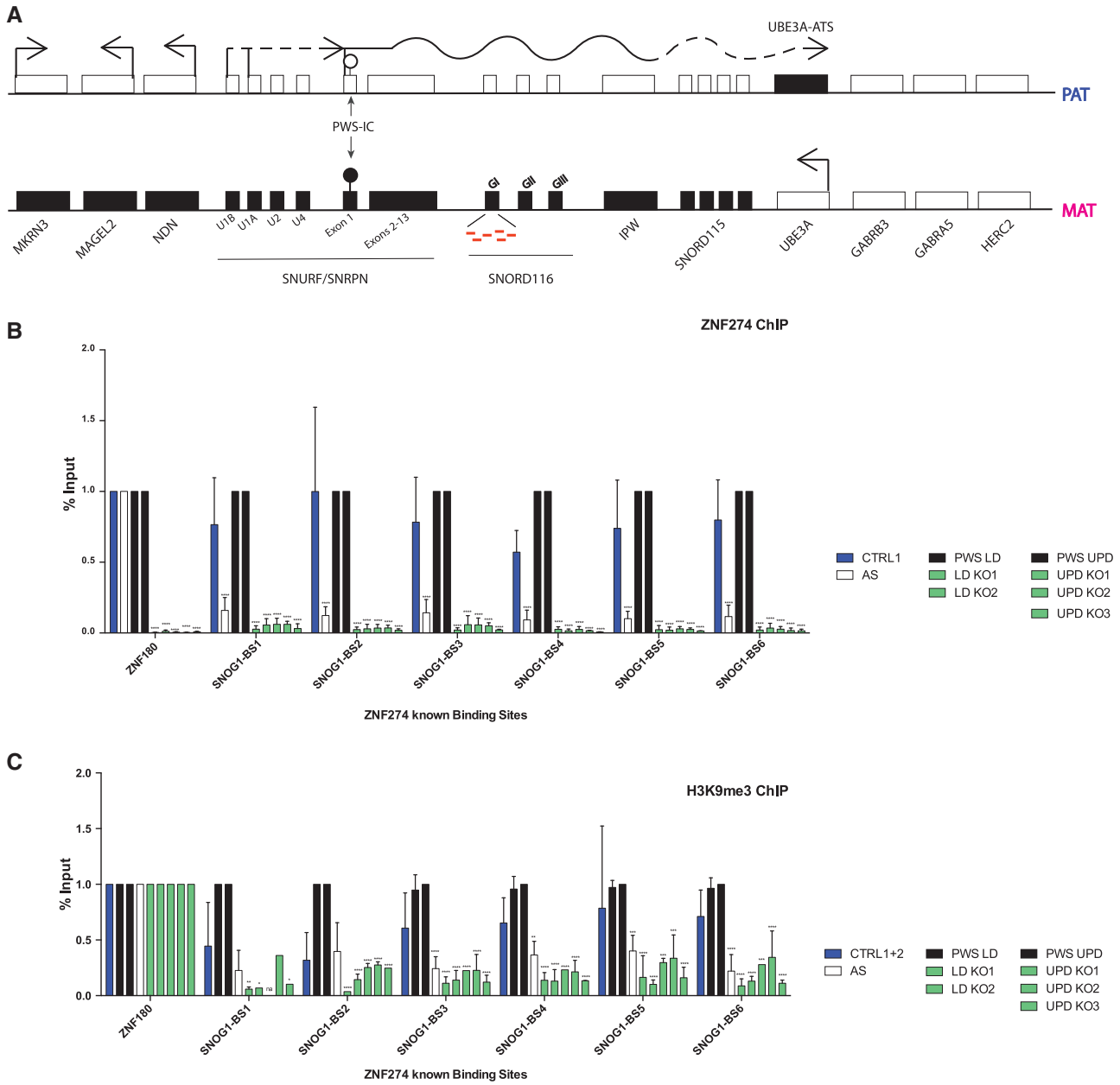

Figure 1. CRISPR/Cas9-mediated Knock-Out of *ZNF274* reduces H3K9me3 and activates *SNORD116* expression in PWS iPSCs. (**A**) Simplified genetic and allelic expression map of 15q11.2-q13. Active and inactive (repressed) transcripts are denoted by open and closed boxes, respectively. Arrows indicate the direction of transcription. A solid black line represents paternal *SNURF/SNRPN* transcripts expressed in most cell types, whereas a dashed black line indicates neuron-specific transcripts, including upstream exons of *SNRPN* and *UBE3A-ATS*. *UBE3A* is maternally expressed in neurons whereas other genes are only paternally expressed in all cell types. The PWS-IC is denoted by the black (methylated)/white (un-methylated) circle. Orange dashes under the *SNORD116* cluster represent the six ZNF274 binding sites within the *SNORD116*s classified as Group 1(19) (*SNOG1-BS1* to *SNOG1-BS6*). (**B**) ChIP assay for ZNF274 in iPSCs. Here and in subsequent figures, PWS patient lines are shown in black, their corresponding *ZNF274* KO lines in green, control (CTRL) cell lines in blue and AS, here used as a negative control, in white. Here and in subsequent figures, quantification of ChIP was performed and calculated as percent input for each sample. Binding at *ZNF180*, a previously reported ZNF274 binding site associated with high levels of H3K9me3 signal, was used as a positive control and, for each line, all other binding sites were normalized to this one. The PWS parental line was set as 1 for each panel and relative normalization to this positive sample was done for each cell line. A minimum of two biological replicates per cell line were performed. Significance was calculated using two-way analysis of variance (ANOVA) test with a Dunnett post-test to compare the two LD KOs to PWS LD and the three UPD KOs to PWS UPD. Here and in subsequent figures, $^{*}P < 0.05$, $^{**}P < 0.01$, $^{***}P < 0.001$, $^{****}P < 0.0001$. (**C**) ChIP assay for the repressive histone modification H3K9me3 in iPSCs. The same color code as in Figure 1B is used for AS, CTRLs, PWS and *ZNF274* KO cell lines.

restores normal levels of expression in neurons after 10 weeks of differentiation (Fig. 3C).

We then examined the expression of transcripts across chromosome 15q11-q13 in iPSC-derived neurons from PWS LD and UPD, their *ZNF274* KO derivatives, CTRLs and the AS LD. Like *116HGG1*, other transcripts (*SNORD116*–1 and *IPW*) within the PWS locus, are expressed in *ZNF274* KO neurons at the same level as those in CTRL neurons (Fig. 4 and Supplementary Material, Table S2). Similar levels of *ZNF274* KO-mediated reactivation of maternal neuronal transcripts are also detected downstream of

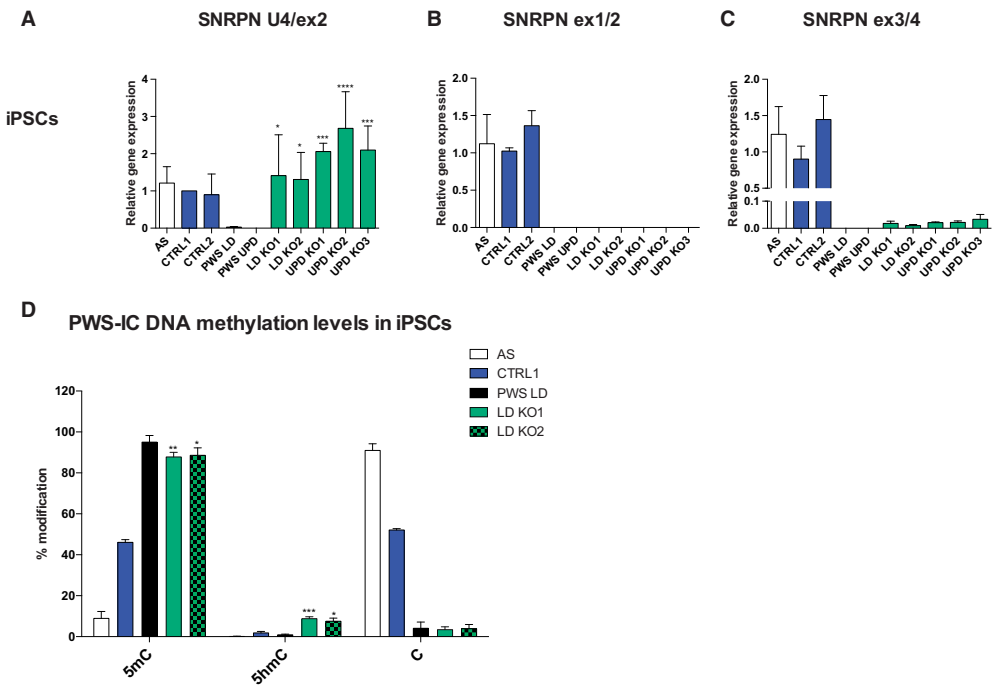

Figure 2. Effect of *ZNF274* KO on *SNRPN* expression and PWS-IC methylation in iPSCs. (**A**) Gene expression of the *SNRPN* U exons (U4/ex2), **(B)** *SNRPN* major promoter (ex1/2) and **(C)** *SNRPN* mRNA (ex3/4) in iPSCs. The same color code as in Figure 1B is used. Here and in subsequent figures, gene expression was assessed using the comparative CT method, *GAPDH* was used as an endogenous control. Data were normalized to CTRL1 for each panel and plotted as the mean with Standard Deviation (SD). A minimum of 3 biological replicates per cell line were performed. Significance was calculated using one-way analysis of variance (ANOVA) test with a Dunnett post-test to compare the two LD KOs to PWS LD and the three UPD KOs to PWS UPD. **(D)** DNA methylation level at the PWS-IC in iPSCs was evaluated using a quantitative restriction endonuclease assay (EpiMark 5hmC and 5mC Analysis Kit) that measures the relative levels of 5-methylcytosine (5mC), 5-hydroxymethylcytosine (5hmC), and unmodified cytosine (C). As expected, CTRL iPSCs show approximately equal levels of 5mC and C at the PWS-IC whereas PWS LD and AS iPSCs display, respectively, almost complete (5mC) and almost no (C) methylation. Although a slight shift from 5mC to 5hmC is apparent, there is almost complete methylation (5mC) of the maternal PWS-IC in the *ZNF274* KO PWS iPSCs. A minimum of 2 biological replicates per cell line were performed. Significance was calculated using two-way analysis of variance (ANOVA) test with a Dunnett post-test to compare the two LD KOs to PWS LD.

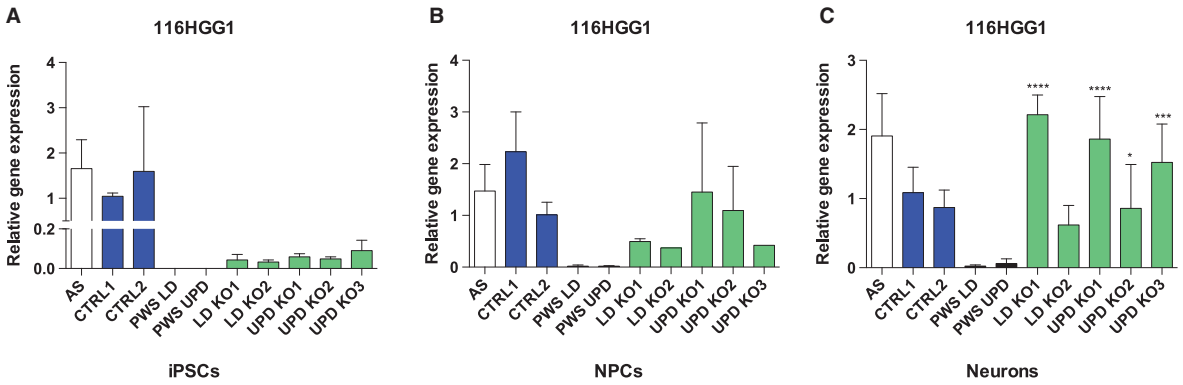

Figure 3. *ZNF274* KO-mediated activation of maternal *116HGG1* transcripts during *in vitro* neurogenesis. Gene expression of the *SNORD116* Host Gene Group I (*116HGG1*) in each cell line through the differentiation process: in (**A**) iPSCs ($n = 3$ minimum), (**B**) 4-week-old neural precursor cells (NPCs) ($n = 1$ minimum) and (**C**) mature 10-week-old neurons ($n = 2$ minimum). The same color code as in Figure 1B is used. Data were normalized to CTRL1 or CTRL2 for each panel and plotted as the mean with Standard Deviation (SD). Significance was calculated using one-way analysis of variance (ANOVA) test with a Dunnett post-test to compare the two LD KOs to PWS LD and the three UPD KOs to PWS UPD.

the PWS locus (*SNORD115–1*, its *115HG* host gene and the antisense overlapping *UBE3A*, *UBE3A-ATS*) (Fig. 4 and Supplementary Material, Table S2). While *ZNF274* KO activates neuronal *UBE3A-ATS* to normal levels, a concomitant decrease in *UBE3A* expression is not observed at least relative to normal control *UBE3A* mRNA levels (Fig. 4 and Supplementary Material, Table S2).

The *SNRPN* U4/exon 2 transcripts are completely rescued by *ZNF274* KO in neurons while *SNRPN* transcripts utilizing exon

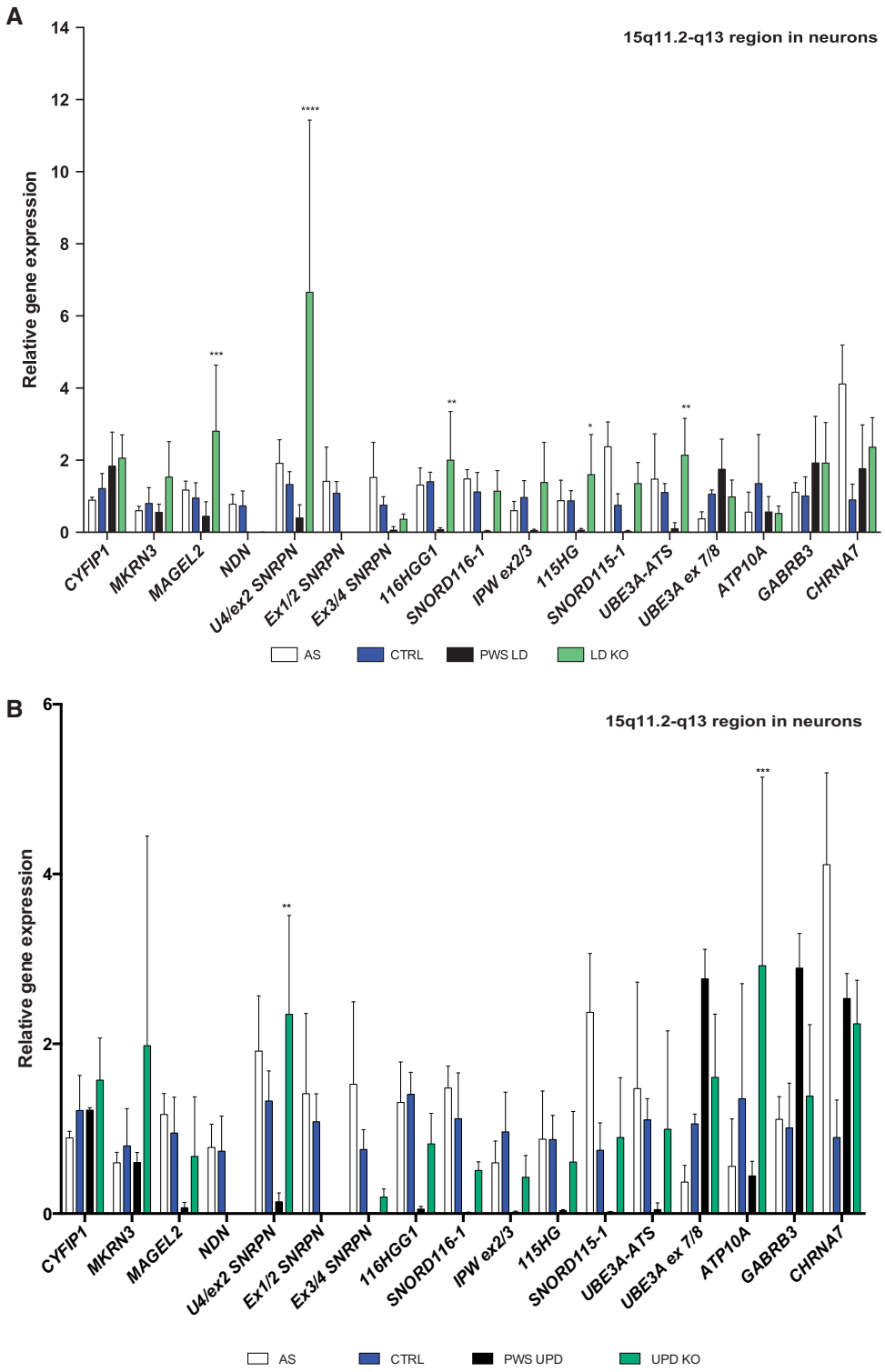

Figure 4. *ZNF274* KO activates transcription in PWS neurons across chromosome 15q11.2-q13. Gene expression of 17 transcripts across the 15q11.2-q13 region in mature 10-week-old neurons. qRT-PCR data was combined from two normal cell lines (CTRLs) and *ZNF274* KO from each parental line: (**A**) LD KOs and (**B**) UPD KOs. The same color code as in Figure 1B is used. Significance was calculated using two-way analysis of variance (ANOVA) test with a Dunnett post-test to compare the combined LD KOs to PWS LD and the combined UPD KOs to PWS UPD.

1 remain silent and exon 3/4 transcripts are partially activated (Figs 4, 5A–C and Supplementary Material, Table S2). These results are consistent with our hypothesis that the ZNF274 complex regulates PWS transcripts via the *SNRPN* upstream promoters. In support of this, higher levels of *SNRPN* U4/exon 2 expression are attained in neurons and NPCs upon *ZNF274* KO than in iPSCs (Fig. 6 and Supplementary Material, Table S2) in accord with the reports that the U1B and U1A promoters are

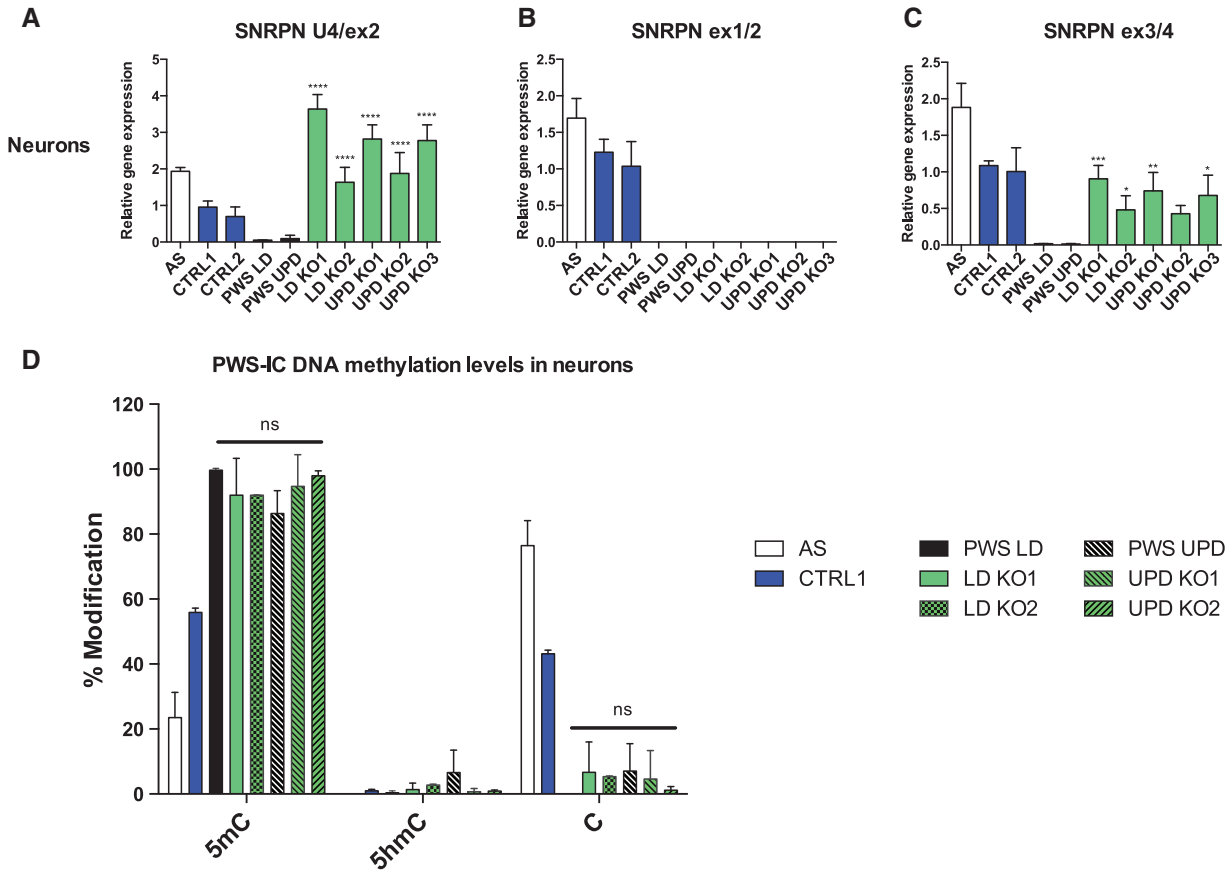

Figure 5. *ZNF274* KO activates *SNRPN* upstream promoters in PWS iPSC-derived neurons without decreasing DNA methylation of the PWS-IC. (**A**) Gene expression of the *SNRPN* U exons (U4/ex2), (**B**) *SNRPN* major promoter (ex1/2) and (**C**) *SNRPN* transcript body (ex3/4) in neurons. The same color code as in Figure 1B is used. Data were normalized to CTRL1 or CTRL2 for each panel and plotted as the mean with Standard Deviation (SD). A minimum of 2 biological replicates per cell line were performed. Significance was calculated using one-way analysis of variance (ANOVA) test with a Dunnett post-test to compare the two LD KOs to PWS LD and the three UPD KOs to PWS UPD. (**D**) DNA methylation level at the PWS-IC in mature 10-week-old neurons evaluated as in Figure 2B. As expected, CTRL neurons show approximately equal levels of 5mC and C at the PWS-IC whereas PWS (LD and UPD) and AS neurons display, respectively, almost complete (5mC) and almost no (C) methylation. There is almost complete methylation (5mC) of the maternal PWS-IC in the *ZNF274* KO PWS neurons. A minimum of 2 biological replicates per cell line were performed. Significance was calculated using two-way analysis of variance (ANOVA) test with a Dunnett post-test to compare the two LD KOs to PWS LD and the UPD KO to PWS UPD.

highly active in the brain (11,12,14). While *ZNF274* KO in PWS LD and UPD neurons activates robust expression of most maternal PWS transcripts (Figs 4, 5A and C, 6 and Supplementary Material, Table S2), there is no change in 5mC levels at the PWS-IC (Fig. 5D), a finding consistent with our observation that *ZNF274* KO does not activate *SNRPN* exon 1 transcription (Figs 4, 5B and Supplementary Material, Table S2) and with our contention that ZNF274 binding to the maternal PWS locus mediates silencing by a mechanism that is independent of the PWS-IC. Our hypothesis is consistent with reports that deletion of the PWS-IC does not result in the loss of imprinted expression in brain (33,34).

Further upstream in the imprinted PWS region, we detect expression of *MAGEL2* and *MKRN3* in PWS LD and UPD neurons and an up-regulation of both upon *ZNF274* KO (Fig. 4 and Supplementary Material, Table S2). *NDN* is not detected in PWS LD and UPD neurons and is not activated by *ZNF274* KO (Fig. 4 and Supplementary Material, Table S2). The latter result would suggest that, like *SNRPN* exon 1 but not other PWS transcripts, *NDN* imprinting is regulated by the PWS-IC, consistent with a mouse model in which deletion of the maternal PWS-IC activated *Ndn* expression (35). *CYFIP1* and *CHRNA7*, genes outside the 15q11-q13 imprinted region, are expressed in neurons derived from all iPSC lines. The mRNA levels of both genes are the same in PWS LD and UPD, and are not affected in their *ZNF274* KO derivatives (Fig. 4 and Supplementary Material, Table S2). Our results suggest a critical role for ZNF274-mediated repression of most neuronal transcripts within but not outside of the imprinted chromosome 15q11-q13 region.

Discussion

The findings summarized here indicate that maternally inherited silent PWS transcripts are activated by CRISPR-mediated knockout of *ZNF274*. Loss of ZNF274 results in a reduction of H3K9me3 within the PWS locus (Fig. 1B and C and Supplementary Material, Fig. S2) and activates expression of maternal transcripts in PWS iPSCs, NPCs and neurons (Figs 1–6 and Supplementary Material, Table S2). Expression of maternal transcripts induced by *ZNF274* KO in PWS neurons attains normal levels and robust activation is observed not only within the PWS locus but also throughout the chromosome 15q11-q13 imprinted region (Figs 3–6 and Supplementary Material, Table S2). Two PWS maternal mRNAs that are not rescued by *ZNF274* KO

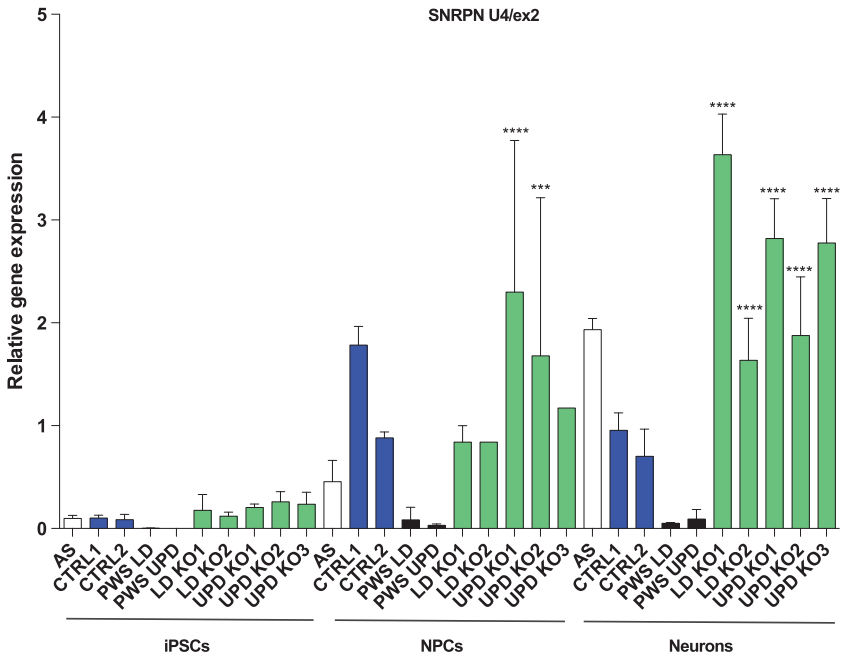

Figure 6. *ZNF274* KO activates *SNRPN* upstream promoters during neuronal differentiation of PWS iPSCs. Gene expression of the *SNRPN* U exons (U4/ex2) in iPSCs, NPCs and neurons. The same color code as in Figure 1B is used. Data were normalized to CTRL1 or CTRL2 neurons for each panel and plotted as the mean with Standard Deviation (SD). A minimum of 3, 1, and 2 biological replicates per cell line for iPSCs, NPCs, and neurons, respectively, were performed. Significance was calculated using one-way analysis of variance (ANOVA) test with a Dunnett post-test to compare the two LD KOs to PWS LD and the three UPD KOs to PWS UPD.

are the *SNRPN* transcript driven by the exon 1 promoter and *NDN* (Figs 2B, 4, 5B and Supplementary Material, Table S2). The most likely explanation in the case of *SNRPN* is that *ZNF274* KO does not alter CpG methylation of the maternal PWS-IC (Figs 2D and 5D) and, hence, does not activate the major *SNRPN* exon 1 promoter. How *NDN* expression is not rescued by *ZNF274* KO is less clear although it has been reported in mouse models that the PWS-IC directly regulates *Ndn* (35). The expression of both MAGEL2 and MKRN3 are up regulated in PWS LD and UPD neurons by ZNF274 KO (Fig. 4 and Supplementary Material, Table S2) suggesting that ZNF274 binding to the *SNORD116* cluster contributes to silencing of maternal alleles by a mechanism that remains to be clarified (Fig. 7).

We did not detect a decrease in the levels of *UBE3A* despite robust activation of *UBE3A-ATS* (Fig. 4 and Supplementary Material, Table S2). One explanation for this is that *UBE3A-ATS*-mediated silencing of *UBE3A* may not be detectable due to the relative immaturity of the neurons differentiated from the iPSCs (25). Another possibility is that the level of expression of the maternal *UBE3A* mRNA is intrinsically higher than that of the paternal allele and thus more resistant to antisense-mediated silencing. In this regard, *UBE3A* expression in both PWS LD and UPD iPSC-derived neurons is increased relative to CTRLs (Fig. 4 and Supplementary Material, Table S2).

In a recent report, the activation of maternal transcripts in human PWS fibroblasts and a mouse model of PWS was demonstrated by using novel compounds that target histone methyltransferase G9a (36). Consistent with our findings, the activation of maternal PWS RNAs via G9a inhibition was associated with reduced levels of H3K9me3 and H3K9me2 at the *SNORD116* locus as well as reduced levels of H3K9me2 at the PWS-IC, without affecting DNA methylation levels at the PWS-IC (36). We show here that, at least in humans, the ZNF274/SETDB1 complex is also required for H3K9me3-mediated silencing of maternal chromosome 15q11-q13 transcripts. While it remains to be determined if the G9a- and ZNF274/SETDB1-histone methylation are mutually independent or complimentary, there appear to be mechanistic differences. For example, *NDN* and *SNRPN* exon 1 are activated by G9a inhibition (36) but not by *ZNF274* KO (Figs 2B, 4, 5B and Supplementary Material, Table S2). This difference could be explained by our observation that the ZNF274/SETDB1 complex specifically regulates brain-specific PWS lncRNA promoters whereas for Kim and colleagues, H3K9me2 reduction at the PWS-IC is responsible for *NDN* and *SNRPN* exon 1 expression, independently of the cell type.

We posit that the ZNF274 complex represses a *cis*-acting regulatory element that is required for initiating transcription from the *SNRPN* U1B and U1A promoters (Fig. 7). The regulatory element repressed by the ZNF274-complex could be an enhancer that activates the *SNRPN* U1B/U1A promoters. Alternatively, the element could be *116HG* lncRNA cloud that functions to regulate the transcription of other genes (37). In our model (Fig. 7), a low level of expression of transcripts driven by the *SNRPN* upstream promoters in *ZNF274* KO iPSCs is upregulated upon neuronal differentiation by brain-specific transcription factors. The activation of normally silent maternal PWS neuronal transcripts in our stem cell knockout model suggests that ZNF274 is a potential target for future therapeutic application in PWS. Our data (Fig. 1B, Supplementary Material, Fig. S2A and B) are consistent with the observation that ZNF274 acts in concert with other ZNF proteins to deposit H3K9me3 at genomic target sites (28). Although *ZNF274* KO would be expected to result in complete loss of H3K9me3 at only about 10% of its target sites (28), genome-wide *ZNF274* KO does not represent a viable strategy since ZNF274 binding does regulate potentially crucial functions outside the PWS locus (38). With this in mind, we are currently characterizing the ZNF274 BS over *SNORD116* in order to specifically block or deplete ZNF274 binding at the PWS locus to

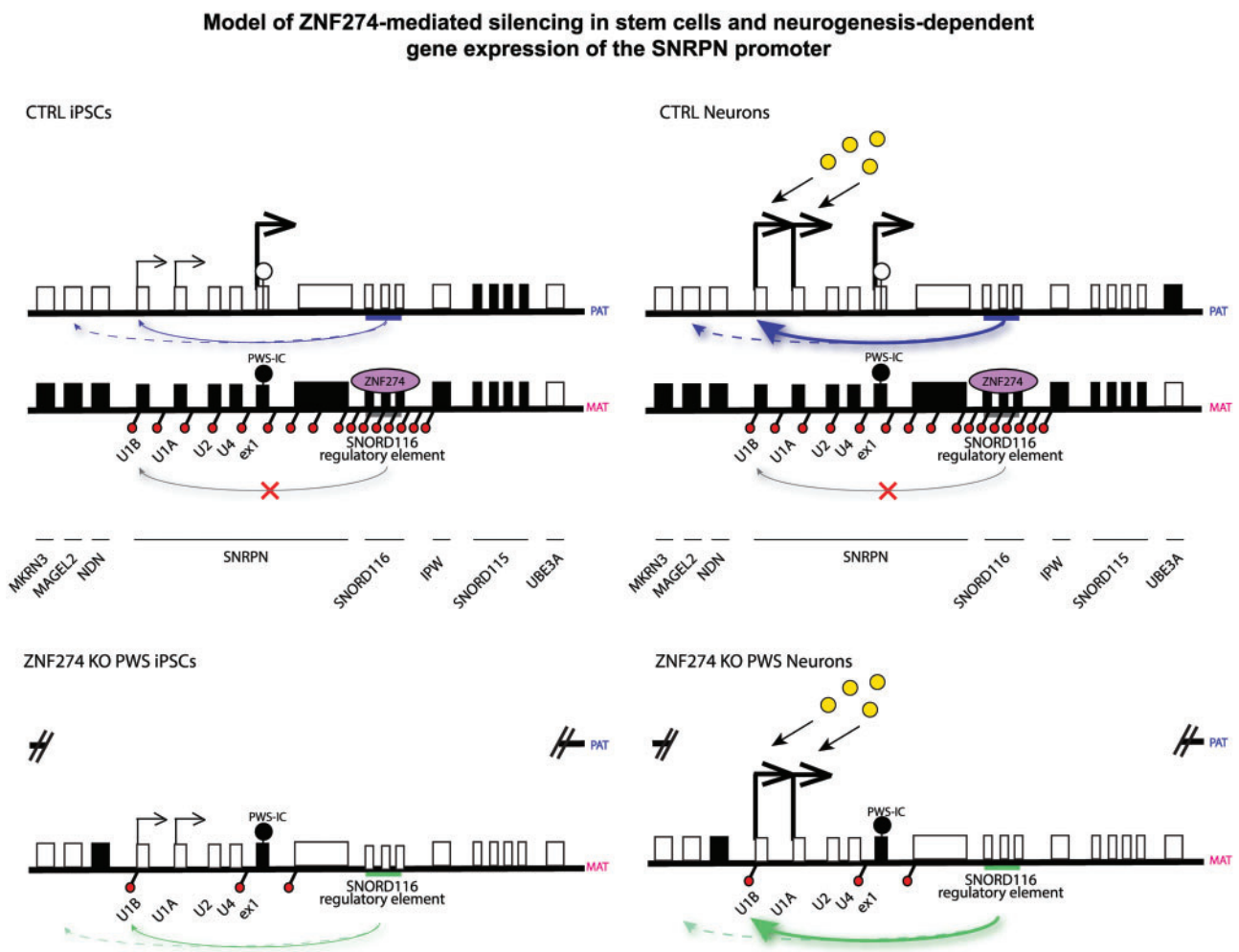

Figure 7. Model of ZNF274-mediated silencing at the PWS locus. Open and closed boxes denote expressed and silenced 15q11.2-q13 genes, respectively, for the CTRL and PWS *ZNF274* KO lines in iPSCs and neurons. The closed (methylated-5mC)/open (un-methylated-C) circles denote the PWS-IC. Arrows indicate the transcription start sites of *SNRPN* (we did not add arrows to other genes for clarity in the figure); thickness is relative to the degree of expression. Genes names are denoted sequentially between the CTRL and PWS *ZNF274* KO lines. Red lollipops represent H3K9me3 signal. ZNF274 is denoted by the magenta ellipse. Colored segment over *SNORD116* represents a putative regulatory element acting in cis on the *SNRPN* upstream exons. Yellow circles represent potential brain specific transcription factors activating the *SNRPN* upstream exons.

reactivate maternal transcripts, offering a potential therapeutic treatment for PWS.

Materials and Methods

Culture conditions of iPSCs and neuronal differentiation

iPSCs were grown on irradiated mouse embryonic fibroblasts and fed daily with conventional hESC medium composed of DMEM-F12 supplemented with knock-out serum replacer, non-essential amino acids, L-glutamine, β-mercaptoethanol, and basic FGF. iPSCs were cultured in a humid incubator at 37 °C with 5% CO_2 and manually passaged once a week (25).

Neuronal differentiation of iPSCs was performed using a monolayer differentiation protocol (39,40) with some modifications (25,26). Briefly, iPSC colonies were cultured in hESC medium for 24h before switching to N2B27 medium. Cells were fed every other day with N2B27 medium containing Neurobasal Medium, 2% B-27 supplement, 2mM L-glutamine, 1% Insulin-transferrin-selenium, 1% N2 supplement, 0.5% Pen-strep and was supplemented with fresh noggin at 500 ng/ml. After three weeks of neural differentiation, neural progenitors were plated on tissue culture plates coated with poly-ornithine/laminin. The neural differentiation medium consisted of Neurobasal Medium, B-27 supplement, nonessential amino acids, and L-glutamine, and was supplemented with 1 μM ascorbic acid, 200 μM cyclic adenosine monophosphate, 10 ng/ml brain-derived neurotrophic factor, and 10 ng/ml glial-derived neurotrophic factor. Unless otherwise specified, cells were harvested once neural cultures reached at least 10 weeks of age.

Lentiviral production, transduction, and clone screening

sgRNAs were designed using a web-based CRISPR design tool and cloned into lentiCRISPR (Addgene Plasmid 49535 and 52961) and lentiGuidePuro (Addgene Plasmid 52963) using our standard protocol (41–43). Lentiviral particles were made by transfecting 293FT cells with 2nd generation packaging systems using Lipofectamine 2000 (Life Technologies). Prior to transduction, iPSCs were treated with 10 μM ROCK inhibitor, Y-27632, overnight. The next day,

iPSCs were singlized using Accutase (Millipore) and transduced with lentivirus in suspension in the presence of 8 μg/ml polybrene in a low-attachment dish for 2 h. Then, the iPSCs/lentivirus mixture were diluted 1: 1 in hESC medium and plated on puromycin-resistant (DR4) MEF feeders at a low density, supplemented with 10 μM ROCK inhibitor, Y-27632, overnight. Attached cells were cultured in hESC medium for an additional 72 h before starting drug selection using puromycin at 0.5 μg/ml during the first week and at 1 μg/ml during the second week. Puromycin-resistant iPSC colonies were individually picked into a new feeder well and screened for indels by performing PCR on genomic DNA and sequencing. The pluripotency of gene edited iPSCs was validated by immunocytochemistry using mouse anti-human stage specific embryonic antigen 4 (SSEA4) and rabbit anti-human OCT3/4, both from Molecular Probes, as previously described (41). Karyotyping and Affymetrix HD 6.0 array were performed by the Genetics and Genomics Division of the UCONN Stem Cell Core. Twenty G-banded metaphase cells from each iPSC line were examined to generate a karyotype for each line.

RNA isolation and RT reaction

RNA was isolated from cells using RNA-Bee (Tel Test, Inc.). Samples were DNase-treated as needed with Amplification Grade DNaseI (Invitrogen) at 37 °C for 45 min, and cDNA was synthesized using the High Capacity cDNA Reverse Transcription Kit (Life Technologies) according to the manufacturer's instructions.

RT-qPCR and expression arrays

For single gene expression assay, expression levels of target genes were examined using TaqMan Gene Expression Assays (Applied Biosystems) on the Step One Plus (ThermoFisher Scientific) or on the BioRAD CFX96 Real Time PCR system (Biorad). An amount of RT reaction corresponding to 30ng of RNA was used in a volume of 20ul per reaction. Reactions were performed in technical duplicates or triplicates and the *GAPDH* Endogenous Control TaqMan Assay was used as an endogenous control, following the manufacturer's protocol. Relative quantity (RQ) value was calculated as $2^{-\Delta\Delta Ct}$ using the normal cell lines CTRL1 or CTRL2 as the calibrator sample.

We designed custom-formatted Taqman low-density arrays (TLDA) with 48 target genes, including two housekeeping genes, allowing for 8 samples (including CTRL2) per card. All primer/probe sets are inventoried in Supplementary Material, Table S2a. Gene expression assays were supplied by Applied Biosystems. For TLDA analysis, 400ng of DNAse-treated RNA was used per RT reaction, according to the manufacturer's directions. cDNA sample, equivalent to 150ng effective RNA, ribonuclease-free water, and PCR master mix were loaded into each TLDA-card fill port. The samples were distributed on the plate by centrifugation. Real-time PCR was performed on the 7900HT or ViiA7 Real-Time PCR systems (Applied Biosystems). We systematically loaded the same CTRL2 sample as our calibrator or Internal Positive Control (IPC) into each card and used the Thermo Fisher Cloud interface to analyse the data with the IPC settings to normalize Cq values across the different plates.

Chromatin immunoprecipitations

ChIP assays were performed as described before (22,44,45). The antibodies anti-ZNF274 (Abnova, Cat# H00010782-M01) and anti-trimethyl histone H3 (Lys9) (H3K9me3; Millipore, Cat# 07–442) were used. Quantification of ChIPs was performed using SYBR Green quantitative PCR. PCR primers used to amplify the purified DNA can be found in Supplementary Material, Table S3. The enrichment of the DNA was calculated as percent input, as described (45). Normal rabbit IgG was used for the isotype controls and showed no enrichment. Data were presented as means with SD and represent the average of at least two biological replicates from independent cultures.

Detection of 5hmC levels

Percentages of 5-methylcytosine (5mC), 5-hydroxymethylcytosine (5hmC) and unmodified cytosine (C) in DNA were assessed using the EpiMark 5-hmC and 5-mC Analysis Kit (New England Biolabs, catalog # E3317S) (22,46,47). qPCR primers used in these assays are denoted in Supplementary Material, Table S3. Reported values represent the average of at least two independent experiments, each analysed in triplicate by quantitative PCR. Data were presented as means and SD of independent experiments.

Statistical tests

Statistical analysis was carried out using Prism software (GraphPad). For each condition shown, averaged values from a minimum of two biological replicates from independent cultures were calculated and the resulting standard deviation (SD) was reported in the error bars. Unless otherwise specified, for each experiment, averaged values for each sample were compared with that of the parental PWS cell line of the same genotype (PWS LD or PWS UPD) and the significance for each un-manipulated vs. KO pair was calculated using the one- or two-way analysis of variance (ANOVA) with the Dunnett post-test.

Supplementary Material

Supplementary Material is available at *HMG* online.

Acknowledgements

We thank David S. Rosenblatt, Gail Dunbar and Daniel J Driscoll for patient clinical evaluation and information, and for providing skin biopsies/fibroblasts. We thank the Jackson Laboratory for Genomic Medicine and the UCONN Health Clinical Research Core for use of their real-time PCR instruments, the UCONN Health Molecular Core and Antoine David, a student in the Magistère de Génétique Graduate Program at Université Paris Diderot, Sorbonne Paris Cité, for their assistance. We also thank Justin Cotney and members of the lab for their helpful discussions and Sourour Mansour and Stormy Chamberlain for critical reading of the manuscript. The contents in this work are solely the responsibility of the authors and do not necessarily represent the official views of the state of Connecticut.

Conflict of Interest statement. The authors declare no competing financial interests.

Funding

Foundation for Prader-Willi Research, CT Regenerative Medicine Fund, Cascade fellowship (M. L.)

Web Resources

UCSC Human Genome Browser, http://genome.ucsc.edu/cgi-bin/hgGateway Web-based CRISPR design tool, http://crispr.mit.edu TIDE: method for easy quantitative assessment of genome editing, https://tide.nki.nl/ CRISP-ID: Detecting CRISPR mediated indels by Sanger sequencing, http://crispid.gbiomed.kuleuven.be/ RoadMap Epigenomics, http://egg2.wustl.edu/roadmap/web_portal/imputed.html#imp_sig. All websites were last accessed on December 12, 2017.

References

1. Angulo, M.A., Butler, M.G. and Cataletto, M.E. (2015) Prader-Willi syndrome: a review of clinical, genetic, and endocrine findings. *J. Endocrinol. Invest.*, **38**, 1249–1263.
2. Cassidy, S.B., Schwartz, S., Miller, J.L. and Driscoll, D.J. (2012) Prader-Willi syndrome. *Genet. Med.*, **14**, 10–26.
3. Chamberlain, S.J. and Lalande, M. (2010) Angelman syndrome, a genomic imprinting disorder of the brain. *J. Neurosci.*, **30**, 9958–9963.
4. Clayton-Smith, J. and Laan, L. (2003) Angelman syndrome: a review of the clinical and genetic aspects. *J. Med. Genet.*, **40**, 87–95.
5. Williams, C.A., Lossie, A., Driscoll, D. and Unit, R. C.P. (2001) Angelman syndrome: mimicking conditions and phenotypes. *Am. J. Med. Genet.*, **101**, 59–64.
6. Buiting, K., Barnicoat, A., Lich, C., Pembrey, M., Malcolm, S. and Horsthemke, B. (2001) Disruption of the bipartite imprinting center in a family with Angelman syndrome. *Am. J. Hum. Genet.*, **68**, 1290–1294.
7. Johnstone, K.A., DuBose, A.J., Futtner, C.R., Elmore, M.D., Brannan, C.I. and Resnick, J.L. (2006) A human imprinting centre demonstrates conserved acquisition but diverged maintenance of imprinting in a mouse model for Angelman syndrome imprinting defects. *Hum. Mol. Genet.*, **15**, 393–404.
8. Ohta, T., Gray, T.A., Rogan, P.K., Buiting, K., Gabriel, J.M., Saitoh, S., Muralidhar, B., Bilienska, B., Krajewska-Walasek, M., Driscoll, D.J. *et al.* (1999) Imprinting-mutation mechanisms in Prader-Willi syndrome. *Am. J. Hum. Genet.*, **64**, 397–413.
9. Shemer, R., Hershko, A.Y., Perk, J., Mostoslavsky, R., Tsuberi, B., Cedar, H., Buiting, K. and Razin, A. (2000) The imprinting box of the Prader-Willi/Angelman syndrome domain. *Nat. Genet.*, **26**, 440–443.
10. Cavaille, J., Buiting, K., Kiefmann, M., Lalande, M., Brannan, C.I., Horsthemke, B., Bachellerie, J.P., Brosius, J. and Huttenhofer, A. (2000) Identification of brain-specific and imprinted small nucleolar RNA genes exhibiting an unusual genomic organization. *Proc Natl Acad Sci U S A*, **97**, 14311–14316.
11. Dittrich, B., Buiting, K., Korn, B., Rickard, S., Buxton, J., Saitoh, S., Nicholls, R.D., Poustka, A., Winterpacht, A., Zabel, B. *et al.* (1996) Imprint switching on human chromosome 15 may involve alternative transcripts of the SNRPN gene. *Nat. Genet.*, **14**, 163–170.
12. Farber, C., Dittrich, B., Buiting, K. and Horsthemke, B. (1999) The chromosome 15 imprinting centre (IC) region has undergone multiple duplication events and contains an upstream exon of SNRPN that is deleted in all Angelman syndrome patients with an IC microdeletion. *Hum. Mol. Genet.*, **8**, 337–343.
13. Landers, M., Bancescu, D.L., Le Meur, E., Rougeulle, C., Glatt-Deeley, H., Brannan, C., Muscatelli, F. and Lalande, M. (2004) Regulation of the large (approximately 1000 kb) imprinted murine Ube3a antisense transcript by alternative exons upstream of Snurf/Snrpn. *Nucleic Acids Res.*, **32**, 3480–3492.
14. Lewis, M.W., Brant, J.O., Kramer, J.M., Moss, J.I., Yang, T.P., Hansen, P.J., Williams, R.S. and Resnick, J.L. (2015) Angelman syndrome imprinting center encodes a transcriptional promoter. *Proc. Natl Acad. Sci. U S A*, **112**, 6871–6875.
15. Meng, L., Person, R.E. and Beaudet, A.L. (2012) Ube3a-ATS is an atypical RNA polymerase II transcript that represses the paternal expression of Ube3a. *Hum. Mol. Genet.*, **21**, 3001–3012.
16. Numata, K., Kohama, C., Abe, K. and Kiyosawa, H. (2011) Highly parallel SNP genotyping reveals high-resolution landscape of mono-allelic Ube3a expression associated with locus-wide antisense transcription. *Nucleic Acids Res.*, **39**, 2649–2657.
17. Rougeulle, C., Cardoso, C., Fontes, M., Colleaux, L. and Lalande, M. (1998) An imprinted antisense RNA overlaps UBE3A and a second maternally expressed transcript. *Nat. Genet.*, **19**, 15–16.
18. Runte, M., Huttenhofer, A., Gross, S., Kiefmann, M., Horsthemke, B. and Buiting, K. (2001) The IC-SNURF-SNRPN transcript serves as a host for multiple small nucleolar RNA species and as an antisense RNA for UBE3A. *Hum. Mol. Genet.*, **10**, 2687–2700.
19. Castle, J.C., Armour, C.D., Lower, M., Haynor, D., Biery, M., Bouzek, H., Chen, R., Jackson, S., Johnson, J.M., Rohl, C.A. *et al.* (2010) Digital genome-wide ncRNA expression, including SnoRNAs, across 11 human tissues using polyA-neutral amplification. *PLoS One*, **5**, e11779.
20. Burnett, L.C., LeDuc, C.A., Sulsona, C.R., Paull, D., Rausch, R., Eddiry, S., Carli, J.F., Morabito, M.V., Skowronski, A.A., Hubner, G. *et al.* (2017) Deficiency in prohormone convertase PC1 impairs prohormone processing in Prader-Willi syndrome. *J. Clin. Invest.*, **127**, 293–305.
21. Polex-Wolf, J., Yeo, G.S. and O'Rahilly, S. (2017) Impaired prohormone processing: a grand unified theory for features of Prader-Willi syndrome? *J. Clin. Invest.*, **127**, 98–99.
22. Cruvinel, E., Budinetz, T., Germain, N., Chamberlain, S., Lalande, M. and Martins-Taylor, K. (2014) Reactivation of maternal SNORD116 cluster via SETDB1 knockdown in Prader-Willi syndrome iPSCs. *Hum. Mol. Genet.*, **23**, 4674–4685.
23. Frietze, S., O'Geen, H., Blahnik, K.R., Jin, V.X. and Farnham, P.J. (2010) ZNF274 recruits the histone methyltransferase SETDB1 to the 3' ends of ZNF genes. *PLoS One*, **5**, e15082.
24. Witzgall, R., O'Leary, E., Leaf, A., Onaldi, D. and Bonventre, J.V. (1994) The Kruppel-associated box-A (KRAB-A) domain of zinc finger proteins mediates transcriptional repression. *Proc. Natl Acad. Sci. U S A*, **91**, 4514–4518.
25. Chamberlain, S.J., Chen, P.F., Ng, K.Y., Bourgois-Rocha, F., Lemtiri-Chlieh, F., Levine, E.S. and Lalande, M. (2010) Induced pluripotent stem cell models of the genomic imprinting disorders Angelman and Prader-Willi syndromes. *Proc. Natl Acad. Sci. U S A*, **107**, 17668–17673.
26. Germain, N.D., Chen, P.F., Plocik, A.M., Glatt-Deeley, H., Brown, J., Fink, J.J., Bolduc, K.A., Robinson, T.M., Levine, E.S., Reiter, L.T. *et al.* (2014) Gene expression analysis of human induced pluripotent stem cell-derived neurons carrying copy number variants of chromosome 15q11-q13.1. *Mol. Autism*, **5**, 44.
27. Martins-Taylor, K., Hsiao, J.S., Chen, P.F., Glatt-Deeley, H., De Smith, A.J., Blakemore, A.I., Lalande, M. and Chamberlain, S.J. (2014) Imprinted expression of UBE3A in non-neuronal

cells from a Prader-Willi syndrome patient with an atypical deletion. *Hum. Mol. Genet.*, **23**, 2364–2373.
28. Imbeault, M., Helleboid, P.Y. and Trono, D. (2017) KRAB zinc-finger proteins contribute to the evolution of gene regulatory networks. *Nature*, **543**, 550–554.
29. Rodriguez-Jato, S., Nicholls, R.D., Driscoll, D.J. and Yang, T.P. (2005) Characterization of cis- and trans-acting elements in the imprinted human SNURF-SNRPN locus. *Nucleic Acids Res.*, **33**, 4740–4753.
30. Sutcliffe, J.S., Nakao, M., Christian, S., Orstavik, K.H., Tommerup, N., Ledbetter, D.H. and Beaudet, A.L. (1994) Deletions of a differentially methylated CpG island at the SNRPN gene define a putative imprinting control region. *Nat. Genet.*, **8**, 52–58.
31. Zeschnigk, M., Schmitz, B., Dittrich, B., Buiting, K., Horsthemke, B. and Doerfler, W. (1997) Imprinted segments in the human genome: different DNA methylation patterns in the Prader-Willi/Angelman syndrome region as determined by the genomic sequencing method. *Hum. Mol. Genet.*, **6**, 387–395.
32. Wawrzik, M., Spiess, A.N., Herrmann, R., Buiting, K. and Horsthemke, B. (2009) Expression of SNURF-SNRPN upstream transcripts and epigenetic regulatory genes during human spermatogenesis. *Eur. J. Hum. Genet.*, **17**, 1463–1470.
33. Bressler, J., Tsai, T.F., Wu, M.Y., Tsai, S.F., Ramirez, M.A., Armstrong, D. and Beaudet, A.L. (2001) The SNRPN promoter is not required for genomic imprinting of the Prader-Willi/Angelman domain in mice. *Nat. Genet.*, **28**, 232–240.
34. DuBose, A.J., Smith, E.Y., Johnstone, K.A. and Resnick, J.L. (2012) Temporal and developmental requirements for the Prader-Willi imprinting center. *Proc Natl Acad Sci U S A*, **109**, 3446–3450.
35. Wu, M.-Y., Jiang, M., Zhai, X., Beaudet, A.L., Wu, R.-C. and Feil, R. (2012) An unexpected function of the Prader-Willi syndrome imprinting center in maternal imprinting in mice. *PLoS One*, **7**, e34348.
36. Kim, Y., Lee, H.M., Xiong, Y., Sciaky, N., Hulbert, S.W., Cao, X., Everitt, J.I., Jin, J., Roth, B.L., Jiang Y.H. (2016) Targeting the histone methyltransferase G9a activates imprinted genes and improves survival of a mouse model of Prader-Willi syndrome. *Nat. Med.*, **23,** 213–222.
37. Powell, W.T., Coulson, R.L., Crary, F.K., Wong, S.S., Ach, R.A., Tsang, P., Alice Yamada, N., Yasui, D.H. and Lasalle, J.M. (2013) A Prader-Willi locus lncRNA cloud modulates diurnal genes and energy expenditure. *Hum. Mol. Genet.*, **22**, 4318–4328.
38. Valle-Garcia, D., Qadeer, Z.A., McHugh, D.S., Ghiraldini, F.G., Chowdhury, A.H., Hasson, D., Dyer, M.A., Recillas-Targa, F. and Bernstein, E. (2016) ATRX binds to atypical chromatin domains at the 3' exons of zinc finger genes to preserve H3K9me3 enrichment. *Epigenetics*, **11**, 398–414.
39. Banda, E. and Grabel, L. (2016) Directed Differentiation of Human Embryonic Stem Cells into Neural Progenitors. *Methods Mol. Biol.*, **1307**, 289–298.
40. Germain, N.D., Banda, E.C., Becker, S., Naegele, J.R. and Grabel, L.B. (2013) Derivation and isolation of NKX2.1-positive basal forebrain progenitors from human embryonic stem cells. *Stem Cells Dev.*, **22**, 1477–1489.
41. Chen, P.F., Hsiao, J.S., Sirois, C.L. and Chamberlain, S.J. (2016) RBFOX1 and RBFOX2 are dispensable in iPSCs and iPSC-derived neurons and do not contribute to neural-specific paternal UBE3A silencing. *Sci. Rep.*, **6**, 25368.
42. Sanjana, N.E., Shalem, O. and Zhang, F. (2014) Improved vectors and genome-wide libraries for CRISPR screening. *Nat. Methods*, **11**, 783–784.
43. Shalem, O., Sanjana, N.E., Hartenian, E., Shi, X., Scott, D.A., Mikkelson, T., Heckl, D., Ebert, B.L., Root, D.E., Doench, J.G. and Zhang, F. (2014) Genome-scale CRISPR-Cas9 knockout screening in human cells. *Science*, **343**, 84–87.
44. Cotney, J.L. and Noonan, J.P. (2015) Chromatin immunoprecipitation with fixed animal tissues and preparation for high-throughput sequencing. *Cold Spring Harb. Protoc.*, **2015**, 191–199.
45. Martins-Taylor, K., Schroeder, D.I., LaSalle, J.M., Lalande, M. and Xu, R.H. (2012) Role of DNMT3B in the regulation of early neural and neural crest specifiers. *Epigenetics*, **7**, 71–82.
46. Doege, C.A., Inoue, K., Yamashita, T., Rhee, D.B., Travis, S., Fujita, R., Guarnieri, P., Bhagat, G., Vanti, W.B., Shih, A. *et al.* (2012) Early-stage epigenetic modification during somatic cell reprogramming by Parp1 and Tet2. *Nature*, **488**, 652–655.
47. Ficz, G., Branco, M.R., Seisenberger, S., Santos, F., Krueger, F., Hore, T.A., Marques, C.J., Andrews, S. and Reik, W. (2011) Dynamic regulation of 5-hydroxymethylcytosine in mouse ES cells and during differentiation. *Nature*, **473**, 398–402.